EXPERIMENTAL AND NUMERICAL ACTIVITIES IN SUPPORT OF THE DESIGN OF ASTRID SODIUM-GAS HEAT EXCHANGER

F.Vitillo, X.Jeanningros, L.Cachon, C.Galati, P.Olympio, and S. Madeleine
CEA Cadarache, Nuclear Energy Division – Department of Nuclear Technology
13108 Saint-Paul-lez-Durance (France)
francescovitillo@hotmail.com; xavier.jeanningros@cea.fr; lionel.cachon@cea.fr;
chiara.galati@cea.fr; paul.olympio@cea.fr ; sylvain.madeleine@cea.fr;

ABSTRACT

In the framework of the development of the ASTRID Sodium-cooled Fast Reactor prototype, the CEA is studying the technical feasibility of adopting a Brayton power conversion cycle to eliminate the sodium-water interaction hazard. Compact heat exchanger technologies are crucial to have reasonable dimensions of the sodium-gas heat exchanger. The CEA is working on several design possibilities, especially in terms of heat transfer pattern and inlet/outlet header geometry. This paper aims to describe the experimental and numerical activities related to these topics. In particular, for the heat transfer patterns, traditional wavy-channel Plate Machined Heat Exchangers (PMHE) as well as an innovative PMHE geometry are studied both numerically and experimentally. The comparison between traditional and innovative PMHE geometries is then shown, to demonstrate that the innovative PMHE is potentially more compact than traditional PMHEs. Regarding the inlet/outlet headers, the adopted calculation methodology is described, characterizing the maldistribution in large channel bundle and adopting a porous media approach to be able to correctly represent the physical phenomena in a reasonably large computational domain.

KEYWORDS
PMHE, Innovative PMHE, CFD, ASST model, LDV, PIV, Maldistribution, Porous Media

1. INTRODUCTION

In the framework of CEA R&D program to develop the Advanced Sodium Technological Reactor for Industrial Demonstration (ASTRID) [1], several thermal-hydraulic studies are ongoing to provide solid technological basis for the use of a Brayton Gas-power conversion system.

The work done at CEA aims to design a first-of-a-kind sodium-gas heat exchanger based on compact technologies. The ASTRID sodium-gas heat exchanger would couple the secondary sodium loop with the tertiary nitrogen loop [2]. This choice is of interest for SFRs since it allows avoiding the energetic sodium-water interaction if a traditional Rankine cycle was used. Given the high mechanical resistance demanded to this component (nitrogen side is supposed to operate at 180 bar [3] whereas the sodium side operates at a few bar), wavy channel Plate Machined Heat Exchangers (hereafter named PMHE) have been identified as suitable candidates for such an application. Hence, a first design has been proposed to identify the critical aspects to investigate further.

The principal challenges when dealing with the gas side of the sodium-gas heat exchanger lies in the heat transfer geometry. In fact, the gas-side determines the global heat transfer coefficient of the Sodium-gas heat exchanger due to its higher thermal resistance compared to liquid sodium. Given that the higher the heat transfer coefficient the higher the compactness of the component, it is worth studying the heat gas-side transfer geometry to have an accurate database on thermal-hydraulic performance of different solutions. On the other hand, the major challenge when dealing with the sodium side is to avoid flow maldistributions. In fact, investigations ongoing at CEA [4] are dealing with a design that aims to avoid gas maldistribution thanks to a high gas-side pressure drop (around 1 bar) and a pressure vessel used as gas header. This is not the case for the sodium side, where a lower pressure drop makes it more sensitive

to maldistribution. Hence the thermal-hydraulic behavior of sodium headers is of primary interest to determine the optimum solution resulting in high thermal efficiency and low thermo-mechanical constraints on the component.
Therefore the present paper aims to describe in detail these challenges as well as the experimental and numerical activities done at CEA in support to the ASTRID sodium-gas heat exchanger design.

2. HEAT TRANSFER GEOMETRY

2.1. Studied Geometries

As already mentioned, wavy channel PMHE have been selected among other compact heat exchanger technologies (i.e. Plate Stamped Heat Exchanger - PSHE, Printed Circuit Heat Exchanger – PCHE i.e. Heatric's, Plate Fin Heat Exchanger - PFHE) due to their high mechanical resistance provided by the diffusion weld of the plates. However, trying to enhance the compactness of this component, an innovative PMHE-based heat transfer geometry has been proposed [5]. Both the traditional and the innovative geometry will be presented hereafter.

2.1.1. PMHE

Nowadays an extensive literature on wavy channel PMHE and PCHE exists (as a few examples see [6-8]). However, the geometrical parameters of a PMHE channel makes it possible to study a wide range of design solutions. Here, a major choice is made: the baseline studied geometry is a wavy channel of squared cross-section. The wavy channel allows a higher heat transfer surface per linear distance between channel inlet and outlet, whereas the squared cross-section is supposed to enhance thermal-hydraulic performance compared to other geometries [9].

2.1.2. Innovative PMHE

Trying to enhance the compactness of the sodium-gas heat exchanger, innovative PMHE-based heat transfer geometry has been proposed [5]. The innovative channel geometry is shown in Figure 1:

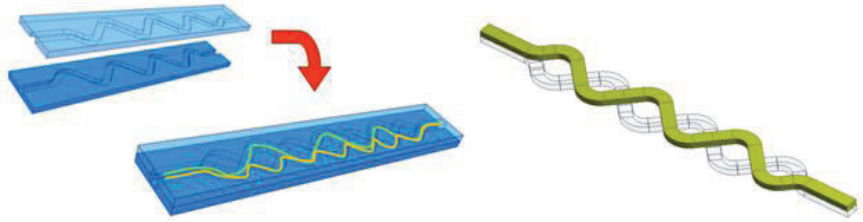

Figure 1 – Superposed channels identification

The channel can be thought as the superposition of two single wavy channels in phase opposition (white and yellow in Figure 1), creating a fully 3D flow. Wavy channels are machined on metal (i.e. any kind of steel) PMHE-type plates. The innovative channel is composed by three elementary geometrical elements i.e. bends, straight channels and mixing zones. If the bends are present in each of the two superposed wavy channels composing the innovative channels, the mixing zone can be thought as the region corresponding to the intersection of the two superposed channels: they can communicate each other through an "open window" called mixing plane. The reference half channel cross section for the innovative channel in the present work is rectangular, with the shorter side equals to half the longer side, i.e. to provide a global squared cross-section. This has been done to easily compare the performance of the innovative and the original PMHE channel.

2.2. Experimental activities

Experimental activities aimed to acquire a wide experimental database on the innovative channel flow, which is much more complex than that of the typical PMHE channel: therefore, once validated the numerical model against experimental data for the innovative channel flow, it is thought it will be possible to correctly describe the PMHE fluid flow too. Three facilities will be described in this paper: a Laser Doppler Velocimetry (LDV) facility, a Particle Image Velocimetry (PIV) facility and a Validation of Heat Exchange in GAS (VHEGAS) facility. The latter has been used to measure the global heat

transfer coefficient both for the PMHE and the innovative channel flow, while the laser velocimetry facilities have been used to acquire a purely aerodynamic database on the innovative channel flow.

2.2.1. LDV Facility

In order to show the primary and secondary fluid motion as well as the boundary layer behavior both for the in-bend and the mixing-zone flow, a LDV has been evaluated as the best measurement technique. In particular, due to its capability to measure boundary layers, a 2-C LDV setup has been used to measure the principal and the radial velocity. The experimental setup has been assembled at the ONERA-Toulouse center. The mockup is shown in Figure 2:

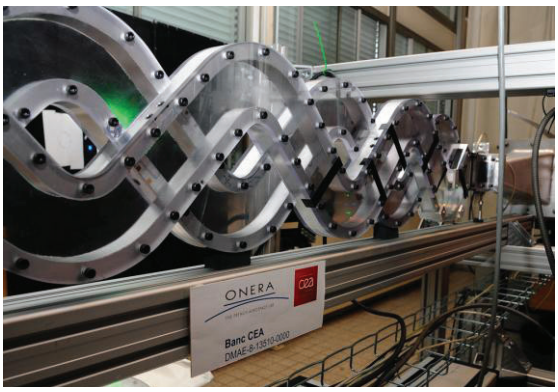

Figure 2 – LDV facility

For sake of brevity, readers can find all the details as well as the evaluation uncertainty in reference [10].

2.2.2. PIV Facility

PIV facility aimed to investigate macroscopic phenomena occurring in the innovative PMHE channel flow. The mockup consists of an entire optical quality PMMA test section.

The channel is designed with an inlet hydraulic diameter of 40 mm, corresponding to an inlet Reynolds number of 12,000. This value is chosen to widen the experimental database, since LDV experiment has been operated with an inlet Reynolds number of 49,700 [10]. The two half channels have a rectangular cross-section of 40mm x 20mm, a corrugation angle of 45°, a 114.6 mm straight distance between two bends and a bend radius of curvature of 57.3 mm. Measurements are done with air at atmospheric pressure and temperature.

The laser used is a double cavity 2x200 mJ pulsed QUANTEL EverGreen 200 YAG Laser, providing a 532 nm (green) light sheet. Its pulse frequency is between 0 and 15 Hz. The camera was a PowerView^{TM} Plus 4MP camera, with a frame-straddling time up to 200 ns. The visualization particles are olive oil droplets. Droplets are created by a "TSI Oil Droplet Generator 9307" atomizer, fed by pressurized air. The average olive oil droplet size map is typically 1 μm. Finally, data acquisition, pre and post-processing is done thank to the "TSI Insight 4G" software.

To evaluate the experimental uncertainty, three types of uncertainty are identified: the uncertainty due to the data acquisition, the uncertainty due to environmental conditions and the uncertainty due to the measurement plane position. The final uncertainty is calculated as the 3σ total uncertainty, where σ is the uniform probability density function standard deviation. Results are provided in Table II:

Table II. Sample table: accuracy of nodal and characteristic methods

	Data acquisition Uncertainty	Environmental conditions Uncertainty	Position Uncertainty	Total 3σ Uncertainty
Vertical velocity fluctuation	0.07 m/s	0. 09 m/s	0. 09 m/s	0.38m/s

2.2.3. VHEGAS Facility

Once obtained the purely aerodynamic database with LDV and PIV, the aim was to measure the global heat transfer coefficient of a heated channel (both PMHE and innovative PMHE). The global heat transfer coefficient is defined as the ratio between the average wall heat flux and the difference between the average wall temperature and the average fluid temperature. Therefore, the Validation of Heat Exchange in GAS "VHEGAS" test-section has been designed in order to obtain these three quantities.

The mockup is composed by two wavy channels of 5 mm height and 10 mm width, a corrugation angle of 20°, a 46.7 mm straight distance between two bend and a bend radius of curvature of 20 mm. The two plates are superposed in phase (i.e. PMHE) or in phase opposition (innovative PMHE). Several holes are present on the mockup's surface to install "1 mm - type K" thermo-couples (TCs) to measure the inlet/outlet fluid temperature and the wall temperature. The channel side and channel top/bottom TCs are located at 1 mm distance from the channel wall. The inlet/outlet TCs are located at channel cross-section center. The mockup is heated by two heating plates, which are placed on the top and bottom surface of the mockup. Note that the two side walls are adiabatic, the mockup being placed into a mineral wool insulating box. Injected thermal power is controlled by a current-controller system.

The flow inlet is given by 7-bar pressurized air underexpanded to atmospheric temperature and pressure to obtain an inlet Reynolds number of around 12,000. A Serv Instrumentation Vortex flow-meter type 8800 is used to measure volumetric flow rate upstream of the mockup. The known flow rate and inlet/outlet temperatures allow for calculation of the thermal power absorbed by the fluid flow. See that this procedure is independent from the actual thermal power provided by the heating plates, which is somewhere lost by test section thermal losses. This thermal power is transferred to the fluid flow by the wall heat flux that can be estimated as the ratio between the calculated absorbed thermal power and the channel wetted surface. The wetted surface value is known thanks to CAD tools. Once the flow is considered as stable, measurements are done by 10 Hz frequency acquisition over five minutes. This frequency is considered as sufficient to statistically analyze the experimental results.

Regarding uncertainty evaluation, a typical standard deviation of such TCs is ±0.5°C with respect to the measured temperature. However, the standard deviation of the set of measured values has to be added to have the total standard deviation σ. The uncertainty is again evaluated as three times the total measured uncertainty. The final 3σ uncertainty are shown in Table III. Note that, the upper values refer to PMHE test case whereas bottom values refer to innovative PMHE test case.

Table III. VHEGAS uncertainty evaluation

	TC-related Standard Deviation	Measurement Statistical Standard Deviation	Mean Value ± Total 3σ Uncertainty
Inlet Temperature	0.5 °C	0.01°C 0.03 °C	44.7± 1.5°C 33.3± 1.5°C
Outlet Temperature	0.5 °C	0.02 °C 0.02 °C	66.7 ± 1.5 °C 67.2 ± 1.5 °C
Mean wall Temperature	0.5 °C	0.03 °C 0.02 °C	72.0 ± 1.5 °C 64.4 ± 1.5 °C
Volumetric Flow Rate	NA	NA	11.6 ± 0.2 m^3/h 11.8 ± 0.2 m^3/h
Innovative PMHE Global heat transfer coefficient	NA	NA	182 ± 27 W/m^2 °C 218 ± 45 W/(m^2K)

2.3. Numerical activities

2.3.1. ASST model description

Aiming to develop a reliable computational model to study the thermal-hydraulic performances of the studied geometries, an innovative Anisotropic Shear Stress Transport (ASST) model is developed and

implemented into the solver ANSYS Fluent 14.5. The formulation of the model utilizes an anisotropic form of the Reynolds stress tensor according to the Caley-Hamilton Theorem, i.e.

$$\overline{\rho u_i' u_j'} = \frac{2}{3}\rho k - \mu_t S_{ij} + \rho C_1 k\tau^2\left(S_{ik}S_{kj} - \frac{1}{3}\delta_{ij}S_{kl}S_{kl}\right) + \rho C_2 k\tau^2\left(\Omega_{ik}S_{kj} + \Omega_{jk}S_{ki}\right) + \\ + \rho C_3 k\tau^2\left(\Omega_{ik}\Omega_{kj} - \frac{1}{3}\delta_{ij}\Omega_{kl}\Omega_{kl}\right) \quad (1)$$

where $S_{ij} = \left(\frac{\partial U_i}{\partial x_j} + \frac{\partial U_j}{\partial x_i}\right), \Omega_{ij} = \left(\frac{\partial U_i}{\partial x_j} - \frac{\partial U_j}{\partial x_i}\right)$ and τ being the turbulent time scale. Usually, for an ω-based model it can be expressed as $\tau = \frac{1}{\beta^*\omega}$, with $\beta^* = 0.09$. Retaining the same approach as [11] and [12] and applying Realizability conditions on the Reynolds Stresses, we obtain:

$$C_1 = \frac{C_{NL1}}{C_{NL4} + C_{NL5}\cdot(\tau S)^3} \quad (2)$$

$$C_2 = \frac{C_{NL2}}{C_{NL4} + C_{NL5}\cdot(\tau S)^3} \quad (3)$$

$$C_3 = \frac{C_{NL3}}{C_{NL4} + C_{NL5}\cdot(\tau S)^3} \quad (4)$$

For the present formulation, value of reference [12] are used, i.e. C_{NL1}=0.8, C_{NL2}=11, C_{NL3}=4.5, C_{NL4}=1000 and C_{NL5}=1. The model is closed by the well-known SST model of Menter [13], where a modification of the eddy viscosity formulation is necessary to take into account the Bradshaw's assumption inside the boundary layer and the new realizable anisotropic formulation of the Reynolds stress tensor. The proposed expression for the eddy viscosity is then:

$$\mu_t = \frac{\rho\,\mathcal{B}}{max\left[\frac{\mathcal{B}}{C_\mu k}\omega, F_2 S\right]} \quad (5)$$

Where $C_\mu = \frac{7.4}{A_1 + \tau S}$, $\mathcal{B} = (a_1 + C_1\tau^2S^2 + C_2\tau^2S^2 + C_3\tau^2S^2)\cdot k$ and $S = \left(\frac{1}{2}S_{ij}S_{ij}\right)^{1/2}$.

Closure coefficients are A_1=3.9 and a_1=0.31. The rest of the model's formulation follows the original SST model with respect to symbols and closure coefficients not mentioned here.

2.3.2. ASST model validation

To validate the selected ASST model, LDV, PIV and VHEGAS facility data are used. For all computation, a velocity inlet (depending to the desired Reynolds number) and a gauge pressure equal to 0 Pa pressure outlet boundary conditions are used. The working fluid is air at atmospheric pressure and temperature (for LDV and PIV measurements) or temperature dependent for VHEGAS data. For the VHEGAS computation, the Simple Gradient Diffusion Hypothesis (SGDH, with a turbulent Prandtl number equal to 0.85) is used to model the turbulent heat flux. The solver is pressure-based one and the coupled pressure-velocity algorithm with pseudo-transient option is used. Gradients are evaluated through the least-squared method. Second order upwind scheme is used for the spatial discretization of momentum, turbulent kinetic energy and turbulent dissipation rate transport equations. Meshing convergence (done for all the three test-cases) has been evaluated by comparing the average wall shear stress on the walls of the channel. Three successively refined meshes (hereafter named as A, B and C according to the refinement level of the near-wall first cell thickness) have been tested. A near-wall approach has been used to obtain proper Y^+ values for the first cell. Table IV shows the results of the convergence evaluation for the LDV geometry:

Table IV. Innovative channel LDV geometry mesh convergence evaluation

Configuration	Y^+	τ_w
A	2.5	1.001 Pa
B	1.2	0.984 Pa
C	0.7	0.988 Pa

See that configuration C shows a converged wall shear stress solution. Based on these trends, we retained configuration C as the reference meshing (difference with B configuration of 0.4%). Note that the same approach in terms of mesh evaluation is used for PIV and VHEGAS channel as well, assuring a good mesh convergence for all the studied geometries.

Experimental data used for validation are: PIV data on the bottom channel middle plane horizontal and vertical velocity fluctuation fields in the last bend; LDV data on bend 0° and 90° cross sections principal and secondary velocity fluctuation profiles; VHEGAS data for the global heat transfer coefficient previously defined. Results are shown hereafter:

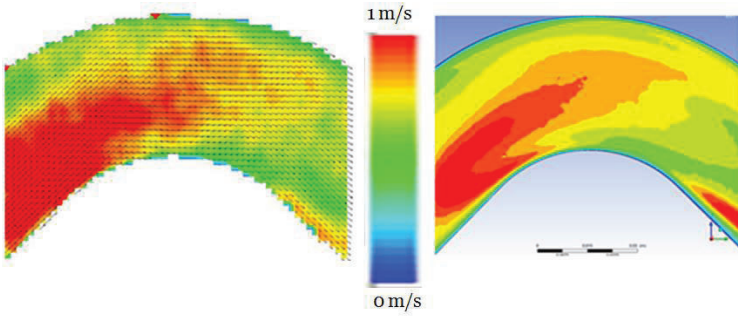

Figure 3 – Bend flow horizontal (up) and vertical (bottom) time-averaged velocity fluctuation comparison between PIV experimental (left field) and ASST (right field) data [m/s]

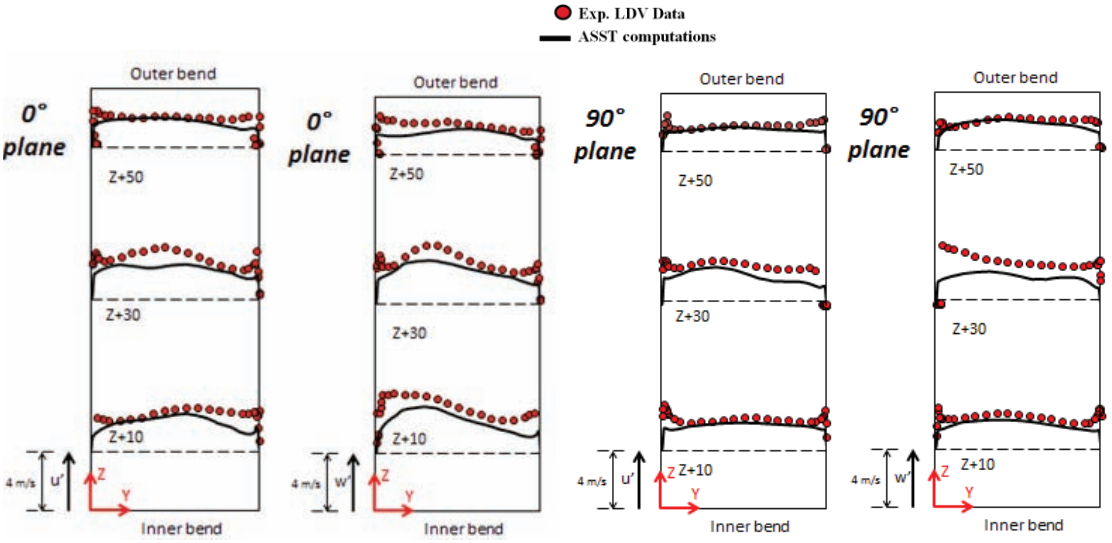

Figure 4 – Bend flow principal (left) and secondary (right) time-averaged velocity fluctuation comparison between LDV experimental (red points) and ASST (black line) results [m/s]

See a general good agreement between experimental data and ASST results. In particular, if discrepancies between PIV and ASST velocity fluctuation fields are easily explained by the high experimental

uncertainties. This is not always the case for LDV-ASST velocity fluctuation profiles. The ASST is capable to reproduce well the velocity fluctuations even when compared with LDV data: discrepancies could be improved by a third order anisotropic formulation of the Reynolds stress tensor, which is supposed to take into account better the flow swirling.
Regarding the thermal validation, the calculation of the numerical heat transfer coefficient is done by applied the evaluated experimental average wall heat flux on the numerical channel wall as an uniform heat flux boundary condition. This heat flux is then divided by the computed temperatures extracted from channel center, to correctly reproduce the experimental measurement. Results of the comparison are shown in Table V:

Table V. VHEGAS and ASST heat transfer coefficient comparison

Studied Geometry	Test Case	h $\left[W/m^2°C\right]$
PMHE	VHEGAS exp. Value	182±27
	ASST computed Value	168
Innovative PMHE	VHEGAS exp. Value	218±45
	ASST computed Value	187

See that the ASST/SGDH computed heat transfer coefficient lies within the experimental uncertainty range. However, see that the computed heat transfer coefficient is generally lower than the measured one. This could be partially explained by the simplicity of the turbulent heat flux model. This is true especially for the innovative channel flow, where the presence of mixing zones makes potentially more difficult to apply a constant turbulent Prandtl number. However, even if the computations underestimated experimental data, this would be conservative with regard to the performance analysis that is shown in the next section.

2.4. Compactness Comparison

Heat transfer performance of different geometries are evaluated on final ASTRID sodium-gas heat exchanger design in terms of compactness, i.e. the ratio between the component thermal power and its total volume. To do that, friction factor and heat transfer correlations are necessary. With the validated ASST/SGDH model it is possible to numerically compute such correlations for a variety of Reynolds number ranges. In the present work the considered range is between 20 000 and 60 000. The working fluid is nitrogen at ASTRID sodium-gas heat exchanger operating conditions [2]. Correlations are studied for three geometries, i.e. the PMHE of squared cross section of 2x2 mm^2 and corrugation angle of 45°, the PMHE of total squared cross section of 2x2 mm^2 (i.e. two superposed wavy channel of 2x1 mm^2) and corrugation angle of 45° and the straight channel case of 2x2 mm^2 squared cross section. The latter is chosen because friction and heat transfer correlations are well-known from literature (i.e. the Blasius correlation for friction and the Dittus-Boelter correlation for heat transfer). A further geometry is studied as well to investigate the real behavior of the innovative geometry (with respect to the simpler geometry of the single channel), i.e. several channels touching each other in already defined mixing zones but also on additional mixing zones created by the superposition of two bends. Hence three innovative channels are modeled and correlations are only obtained for the middle channel, where the effect of lateral channels is clearer. Found correlations [14] are listed in Table VI. The maximum standard errors for the shown pressure drop and heat transfer correlations are respectively 0.003 and 3.5.

Table VI. Friction factor and heat transfer correlations

Geometry	Friction factor correlation	Heat transfer correlation
Straight tube	$f = 0.316Re^{-0.25}$ *(Blasius)*	$Nu = 0.023Re^{0.8}Pr^{0.4}$ *(Dittus Boelter)*
PMHE α =45°	$f = 3.117Re^{-0.337}$	$Nu = 0.0513Re^{0.7471}Pr^{0.4}$
Innovative PMHE α =45°	$f = 0.8388Re^{-0.154}$	$Nu = 0.0364Re^{0.789}Pr^{0.4}$
Triple Innovative PMHE α =45°	$f = 0.5351Re^{-0.078}$	$Nu = 0.0377Re^{0.7787}Pr^{0.4}$

Reference heat exchanger performances are taken from ASTRID sodium-gas heat exchanger are:

- Module Thermal Power: 24 MWth;
- Gas-side pressure drop: 1 bar;
- Sodium Inlet Temperature: 530 °C
- Gas Inlet Temperature: 310°C
- Sodium mass flow rate: 99 kg/s
- Gas mass flow rate: 101 kg/s

Results are of the compactness comparison for ASTRID sodium gas heat exchanger conditions are shown in Table VII.

Table VII. Compactness comparison of different geometries for ASTRID Sodium-Has Heat Exchanger conditions (plate width = 1 m)

	Straight channel	PMHE channel 45°	Single innovative channel 45°	Triple innovative channel 45°
Compactness [MW/m^3]	**20**	**23**	**28**	**27**
Total number of plates [-]	**138**	**320**	**420**	**474**
Inlet/Outlet straight distance [m]	**2.36**	**0.91**	**0.58**	**0.54**

The innovative channel geometry presents always the higher compactness. The code-estimated improvement is as high as 40% for the 45° case when compared to the straight channel case. The innovative channel compactness improvement is even more impressive when looking at the PMHE, which is an existing technology more and more used in the industry when dealing with heat exchangers. The major parameter of interest for a compact heat exchanger is therefore the heat transfer surface to volume ratio, which is higher for the innovative channel, as shown by the hydraulic diameter evaluation. Hence it is clear that the interest given by the innovative geometry is due to the fact that the global length has to be reduced to meet a pressure drop value, reducing the total volume of the component keeping the right heat transfer surface.

3. MALDISTRIBUTION AND HEADERS DESIGN FOR LARGE CHANNEL BUNDLE

Thermal-hydraulic and thermo-mechanical sizing of the channel bundle is conventionally made under a perfect distribution hypothesis: each channel is supplied with the same mass-flow. However, distribution cannot be perfect and sizing hypothesis might be invalidated because of channel supply imbalance. Hence, heat-exchanger design has to be ensured in that imbalance in mass-flow distribution is low enough to validate bundle sizing. In heat-exchanger architecture this function is dedicated to the headers.

3.1. Maldistribution characterization and effects

This study is focusing on Na/N_2 exchange modules. Each module is supposed to be made up of 9000 sodium channels. Supply imbalance means that each channel is supplied with its own mass-flow m_i. Hence, the first way to characterized maldistribution is to determine the mass-flow standard deviation σ of the 9000 channels. This information is useful since it allows comparing distribution cases. However it gives no direct information about the imbalance acceptability.

Since each channel is supposed to be supplied with its own mass-flow, the global exchanged power ϕ has to be re-evaluated. This global exchange power can be considered as the discrete sum of each exchanged power between couples of Na/N_2 channels ϕ_i.

$$\phi = \varepsilon\, \dot{C}_{min}\, (Te_{Na} - Te_{N2}) = \dot{C}_{Na}(Te_{Na} - Ts_{Na}) = \dot{C}_{N2}(Ts_{N2} - Te_{N2}) = \sum_i \phi_i \quad (6)$$

$$\phi_i = \varepsilon_i\, \dot{C}_{i\,min}\, (Te_{Na} - Te_{N2}) \quad (7)$$

Hence the notion of local effectiveness ε_i can be introduced. Heat exchange effectiveness, local or global, mainly depends on the kind of exchanger (counter flow, coaxial…) and the mass-flow. It is calculated using NTU method [15]. As inlet temperatures are imposed, ϕ_i can be easily calculated. Assuming the mass-flow in each channel is known, then the channel outlet temperature can be found. Ignoring heat flux between Na channels (respectively N_2 channels), outlet temperature per channel Ts_i could be written as:

$$Ts_{i\ Na} = Te_{Na} - \frac{\phi i}{\dot{C}_{Na}} \quad (8) \qquad Ts_{i\ N2} = \frac{\phi i}{\dot{C}_{N2}} - Te_{N2} \quad (9)$$

As each channel is supplied with a different mass-flow, outlet temperature for each channel will also be different. This temperature difference between channels leads to the main problems induced by maldistribution. Firstly, it will generate differential dilations in the bundle, inducing thermal stress. One way to measure influence of these differential dilations on bundle's mechanical behavior is to lead thermomechanical calculation, considering outlet temperature of each channel. Secondly, maldistribution could have an impact on global effectiveness. To this purpose, a linear mixing law to compute the mean temperature in outlet header can be used. Indeed, only monophasic sodium flow is considered.

$$Ts = \frac{\sum_i^n Ts_i\ \dot{m}_i\ Cp_i\ (Ts_i)}{\sum_i^n \dot{m}_i\ Cp_i(Ts_i)} \quad (10)$$

Once mean temperature in outlet header is known, heat exchanger's global effectiveness is evaluated [15] as:

$$\varepsilon = \frac{\max\ (Ts_{Na} - Te_{Na}, Ts_{N2} - Te_{N2})}{\Delta T_{max}} \quad (11)$$

Given the above, the four necessary criteria to estimate maldistribution influence are identified. Standard deviation of channel mass-flow allows comparing distribution cases two by two. Outlet temperature per channel provides thermal cartography of the bundle. This cartography is required to validate thermomechanical behavior. Outlet header mean temperature and global effectiveness are required to validate thermal-hydraulic behavior of the exchanger. Lalot [16], propose another quantity to estimate maldistribution influence, i.e.:

$$\eta = \sqrt{\frac{\frac{1}{2}\rho {v_0}^2 + \Delta p_{av}}{\Delta p_{av}}} \quad (12)$$

This formulation provides a first design rule. Indeed, it traduces the fact that maldistribution is due to imbalance between dynamic pressure ($\frac{1}{2}\rho {v_0}^2$), function of v_0, the sodium header inlet mean velocity, and the bundle pressure loss Δp_{av} between inlet and outlet headers.

3.2. Header design

According to the expression of η, there are only two variables to correct maldistribution phenomena: v_0 and Δp_{av}. Each module is supplied with 100kg/s of sodium. As cavitation effects and piping bulk in the pressure vessel have to be limited, v_0 is limited at 10m/s. On the other side, active domain of the channel bundle is sized to achieve the desired heat exchange performance and mechanical behavior. Hence, one way to minimize η is to add pressure drop between header inlet and the active domain of the bundle. To tune the pressure drop addition needed, designer first has to fix header geometry. Once the header's fluid domain is known, CFD can be used to compute mass-flow per channel.

3.2.1. Modeling maldistribution for large channel bundle

The considered bundle consists of 9000, 3 x 6 mm² channels, approximately 3.4 m long between inlet and outlet headers for the simplest studied geometry, i.e. PMHE with straight channels both on the gas and the sodium side. In case of perfect distribution, Reynolds number in channel is about 9 500. Evaluating mass-flow in each of these channels mainly consist in a good description of bundle pressure loss. As each channel is differently supplied, a first estimation is that an explicit CFD calculation needs about 2.3

billion elements. In the framework of this project phase it was worth considering as many elements as possible. Hence, a first mechanical design of the header shows that CFD computation could be done considering only ½ to 1/8 of the bundle; depending on the header type and allowed symmetry conditions. But this is still not enough, because the mesh would still be too heavy to be dealt in project phase.

The main axis of this study was to use porous media to impose bundle pressure drop allowing a rescaling of the modeled bundle. This rescaling consists in reducing the bundle form 3.4 m to 3. 10^{-2} m. Since the mass-flow for each channel will be investigated, their cross-section has to be conserved. Hence our model consists of 9000 channels defined as porous media with unit porosity. Imposed pressure drop in these porous media mainly corresponds to wall losses. In fact, CFD calculations as well as Idel'cick [17] correlation show that, in our case, singular pressure drop are negligible compared to wall losses. For example, using CFD calculations, it was not possible to distinguish singular pressure drop from wall losses in case of a realistic distribution. To conclude, porous media imposed friction pressure drop is determined using Blasius correlation.

To do that, pressure drop in the porous media is computed from the element velocity field by the addition of a momentum source term to the standard fluid flow equations. CFD commercial codes offer different formulations in this purpose. A power law formulation is used; therefore the source term is modeled as a power law of the velocity magnitude ($|v|$ [m/s]):

$$S = -C_0|v|^{C_1} \quad (13)$$

C_0 and C_1 can be easily determined from Blasius correlation. This formulation is isotropic, but this is not disturbing since our mesh includes channel section and walls. The main interest of this formulation is that it could cover a wide range of Reynolds numbers. The only limitation comes from Blasius correlation itself. So it allows computing most of imbalance distribution case with a constant precision.

For calculations presented here, turbulence is modeled by the High-Reynolds two equation realizable k-ε model [18]. Hence the aim is to have a y+ at least equal to 30 in most of our geometry (channels included). For each calculation, convergence is ensured looking at absolute residuals (10^{-5} for all transported variables), as well as mass-flow standard deviation of the channels and minimum/maximum facet velocity measured in channels.

The presented method has been validated considering a half plate of the module, i.e. 63 channels (Figure 5). Firstly the pressure drop for each channel has been compared with Blasius correlation, ensuring that wall losses dominate total losses of the bundle and hence validating the use of Eq. (13) for porous media imposed pressure drop.

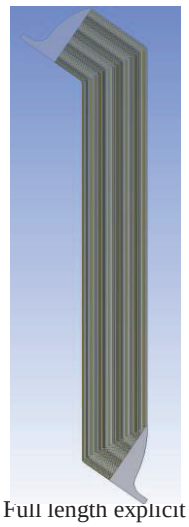

Full length explicit 63 channels bundle (3.4m)

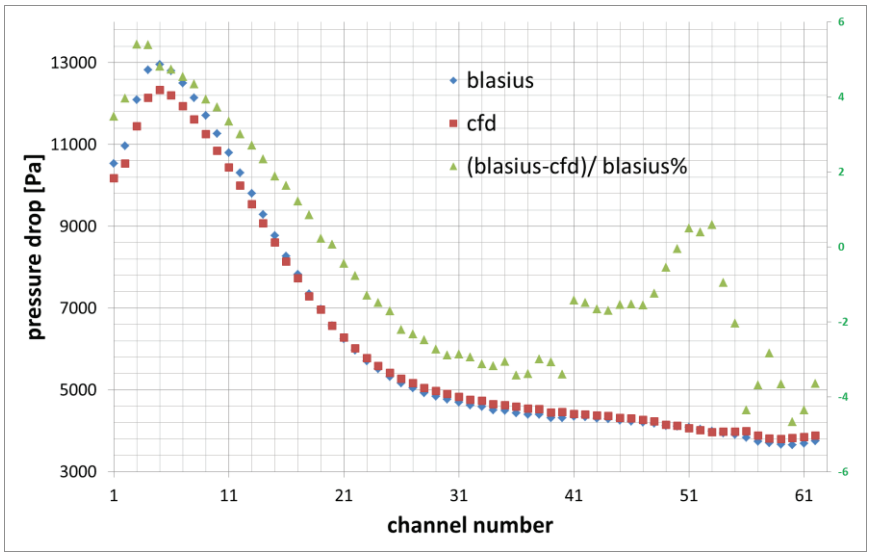

Pressure drop per channel comparison : CFD versus Blasius

Figure 5 - Results on test geometry

Then the 63 mass-flow obtained with the explicit model are compared to the ones obtained with porous media (Figure 6). Observe that the porous media model reproduce the mass-flow distribution with global difference less than 5%.

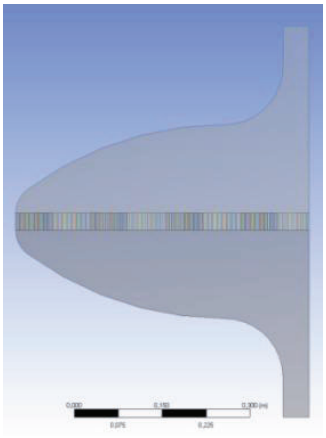

Rescaled porous 63 channels bundle (3 10^{-2}m)

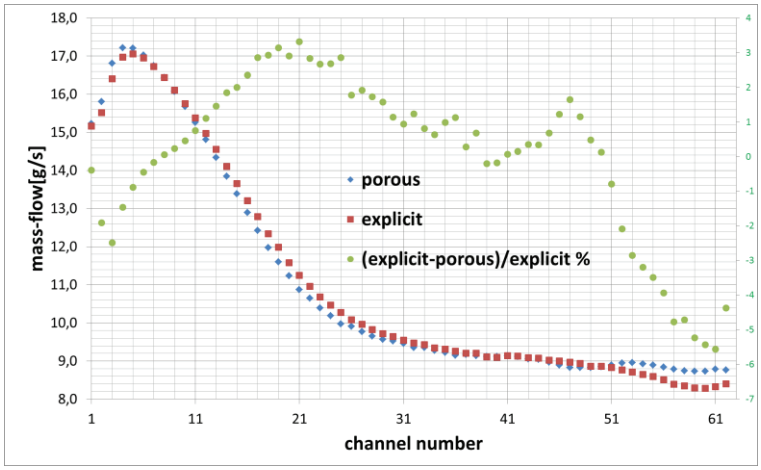

Mass-flow per channel comparison : explicit model versus porous

Figure 6 - Results on rescaled geometry compare to test geometry

3.2.2. Results on realistic geometry

Once the porous media method established, it is used for a bigger geometry, representative of the bundle and the headers. Two kinds of header are studied: compact header is the most consistent with design constraints, whereas U-type corresponds to a more classical design for plate heat-exchangers.

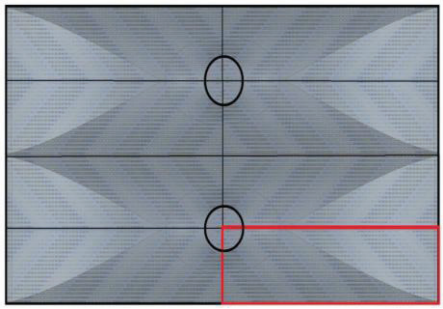

Compact header (view from the top)

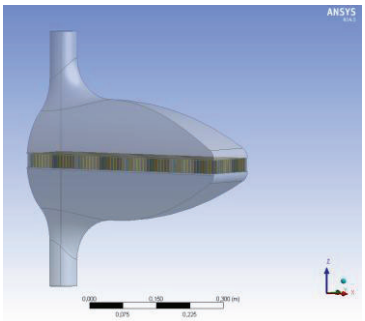

1/8 Compact header with 1125 rescaled channels

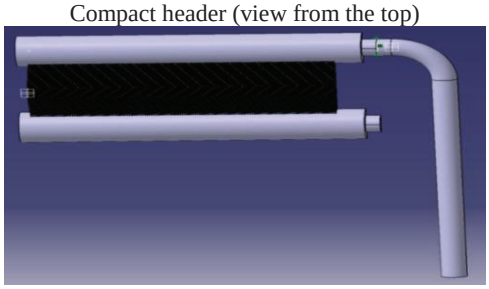

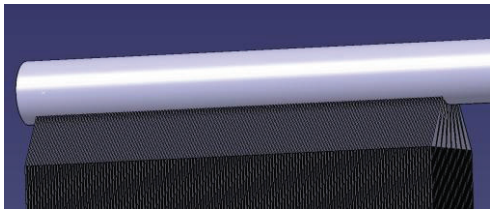

U-type header with 9000 rescaled channels

Figure 7 - Studied headers (fluid domain)

Complete post-treatments, based on previous criteria, are summarized in the Table VIII for three distribution cases. The first one corresponds to compact header as design Figure 7. The second

corresponds to the optimized compact header. This optimization consists in putting mixing grid between the header inlet and the bundle. The third case corresponds to U-type header as described in Figure 7. Applying the methodology presented in section 3.2.1., the mass-flow in each channel is post-treated to obtain the 3D plot shown in Figure 8. To illustrate methodology's potential, only two of the worst encountered distribution and a well-balanced distribution are considered here. Note that no definitive solution and design of the header in this paper will be provided in this paper.

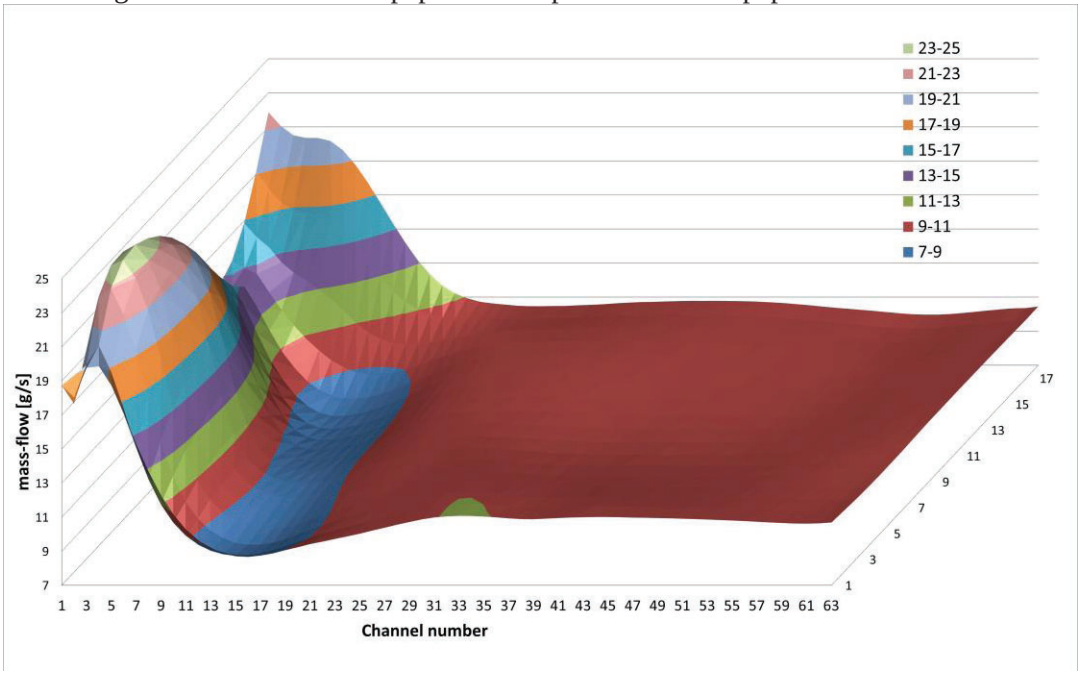

Figure 8 - Non-optimized compact header: Mass-flow [g/s] per channel

From the methodology presented in paragraph 3.1, a first temperature cartography of the bundle can be provided, to perform a conservative thermo-mechanical sizing of the component. Note that, since the thermal flux between Na channels, respectively N_2 channels, is neglected, temperature difference between channels is slightly overestimated. Also, maldistribution influence on effectiveness and bundle's thermal cartography is overestimated too. In the framework of design and sizing project phase, this methodology is particularly interesting as it is conservative.

Table VIII. Results

			Compact header	Optimized Compact header	Type U	ideal distribution
Mean velocity header inlet	v_0	[m/s]	10	10	10	-
ΔP	Δp_{av}	[Pa]	6000	13400	9000	-
Standard Deviation	σ	[%]	25	3	25	0
Peak mass-flow	$\dot{m}_{min}/\dot{m}_{mean}$	[%]	70	92	13	100
	$\dot{m}_{max}/\dot{m}_{mean}$	[%]	215	108	124	
Outlet Na temperatures	Ts_{na}^{mean}	[°C]	348	345	354	345
	Ts_{na}^{min}	[°C]	314	334	310	
	Ts_{na}^{max}	[°C]	437	355	374	
Effectiveness	ε	[-]	0.91	0.93	0.89	0.93

The highlight of the Table VIII is that maldistribution not only depends of v_0 and Δp_{av}. Indeed, for two kind of header, standard deviation σ remains the same even if v_0 and Δp_{av} change. The standard deviation

is also representative of effectiveness ε only when comparing the same kind of header. On the other hand, standard deviation could have the same value (25%) even when the impact on effectiveness is different (from 2.6% to 5%). This depends on header's geometry. Regarding peak mass-flow, observe again that standard deviation does not distinguish between over-supplied or under supplied channel.

4. CONCLUSIONS

In the framework of the development of the ASTRID Sodium-cooled Fast Reactor prototype, the activities in support of the development of the sodium-gas heat exchanger are presented. The experimental means as well as the validated CFD model allow for a fine study of the thermal-hydraulic behavior of standard wavy channel PMHE as well as of an innovative PMHE. Results show that compactness can be potentially improved if the new proposed geometry is adopted.

With regard to the sodium side, the major problem to be faced is the flow maldistribution in headers. To study this problem, the used methodology is presented: it has been shown that it is possible to model the channel bundle as a porous medium while keeping a finer mesh inside inlet and outlet headers. This procedure, validated against available pressure drop correlations, does not result in an excessively demanding computational domain.

The shown thermal-hydraulic activities will support the final design of ASTRID sodium-gas heat exchanger. Demonstrating the technical feasibility of the Brayton power conversion system will likely be of primary importance for future public acceptance of SFRs.

NOMENCLATURE

U_i	m/s	Mean velocity along the x_i axis
u_i'	m/s	Velocity fluctuation along the x_i axis
k	m^2/s^2	Turbulence kinetic energy
ω	s^{-1}	Specific dissipation rate
$\dot{C}_{N2}$	$J.C^{-1}.s^{-1}$	Nitrogen flow stream heat capacity rate
$\dot{C}_{Na}$	$J.C^{-1}.s^{-1}$	Sodium flow stream heat capacity rate
$\dot{C}_{min}$	$J.C^{-1}.s^{-1}$	$\dot{C}_{min} = min(\dot{m}_{Na}Cp_{Na}; \dot{m}_{N2}Cp_{N2})$
$Ts_{i\ N2}$	°C	Inlet local nitrogen temperature for the channel i
$Ts_{i\ Na}$	°C	Outlet local sodium temperature for the channel i
$\dot{m}_{N2}$	Kg/s	Nitrogen mass-flow
$\dot{m}_{Na}$	Kg/s	Sodium mass-flow
ΔT_{max}	°C	$= \max(Te_{Na}; Te_{N2}; Ts_{Na}; Ts_{N2}) - min(Te_{Na}; Te_{N2}; Ts_{Na}; Ts_{N2})$
Δp_{av}	Pa	Channel bundle pressure drop
Cp_{N2}	$J.kg^{-1}.C^{-1}$	Nitrogen specific heats
Cp_{Na}	$J.kg^{-1}.C^{-1}$	Sodium specific heats
Te_{N2}	°C	Inlet nitrogen temperature
Te_{Na}	°C	Inlet sodium temperature
Ts_{N2}	°C	Outlet global nitrogen temperature
Ts_{Na}	°C	Outlet global sodium temperature
v_0	m/s	Header inlet mean velocity
ε_i	-	Local effectiveness
ϕ_i	W	Local exchange power between a couple of Na/N2 channel
S	Pa/m	Source term
ε	-	Global effectiveness
ρ	Kg/m^3	fluid density
ϕ	W	Global exchange power

ACKNOWLEDGMENTS

This work, associated to the technological development of the sodium gas heat exchanger, is supported by the ASTRID CEA team project, and the CEA SFR R&D project.

REFERENCES

1. E.Abonneau et al., "The ASTRID Project: Status and Prospects towards the Conceptual Design Phase", *Proceeding of the International Conference on the Advances of nuclear Power Plants 2014 – ICAPP'14*, Charlotte, USA, April 6-9, 2014, Paper 14116, pp. 447-455
2. L.Cachon et al., "Innovative Power Conversion System for the French SFR Prototype, ASTRID", *Proceeding of the International Conference on the Advances of nuclear Power Plants 2012 – ICAPP'12*, Chicago, USA, June 24-28, 2012, Paper 12300, pp. 538-552
3. E.Saez et al., "The use of gas-based energy conversion cycles for sodium fast reactors", *Proceeding of the International Conference on the Advances of nuclear Power Plants 2008 – ICAPP'08*, Anaheim, USA, June 8-12, 2008, Paper 8037, pp. 565-573
4. CACHON et al., "Echangeur de chaleur à plaques à échange thermique et compacité améliorés", PATENT n°HD14482, 2014
5. F.Vitillo, "*Experimental and Numerical Contribution to heat transfer enhancement in compact plate heat exchangers*", PhD Thesis, ISAE, Toulouse (FR), November 2014
6. D.E. Kim et al., "Numerical Investigation on thermal-hydraulic performance of new printed circuit heat exchanger model", *Nuclear Engineering and Design* **238 (**12), pp.3269-3276, December 2008
7. I.H.Kim et al., "Thermal hydraulic performance analysis of the printed circuit heat exchanger using a helium test facility and CFD simulations", *Nuclear Engineering and Design* **239 (**11), pp.2399-2408, November 2009
8. I.H.Kim, H.C.No, "Thermal hydraulic performance analysis of a printed circuit heat exchanger using a helium-water test loop and numerical simulations", *Applied Thermal Engineering* **31**, (17-18), pp.4064-4073, December 2011
9. T.Schmerber, "*Calculs CFD sur des échangeurs thermiques Sodium/Gaz pour ASTRID*", MSc Thesis, UTBM – Université de Belfort (FR), 2011
10. F.Vitillo et al., "Turbulence Model Comparison for Innovative Compact Plate Heat Exchanger Design Application", *Proceeding of the International Conference on the Advances of nuclear Power Plants 2014 – ICAPP'14*, Charlotte, USA, April 6-9, 2014, Paper 14143, pp. 648-657
11. T.H.Shih, J.Zhu and J.L.Lumley, "*A realizable Reynolds Stress algebraic equation model*", NASA TM 105993, 1993
12. E.Baglietto, H.Ninokata, T.Misawa "CFD and DNS methodologies development for fuel bundle simulations", *Nuclear Engineering and Design* **236**, pp.1503-1510 (2006)
13. F.R.Menter, "Two equation eddy viscosity turbulence models for engineering applications", *AIAA Journal* **32** (8), 1994
14. F.Vitillo et al., "An innovative Plate Heat Exchanger of Enhanced Compactness", *Applied Thermal Engineering*, doi:10.1016/j.applthermaleng.2015.05.019
15. Ramesh K. Shah and Dušan P. Sekulic, "Fundamentals of Heat Exchanger Design", 2003 John Wiley & Sons, Inc.
16. S.Lalot , P.Florent, S.K.Lang, E.Bergles, "Flow mal-distribution in heat exchangers Applied Thermal Engineering" 1998
17. I.E.Idel'cik, "Memento des pertes de charge", Eyrolles Paris 1979
18. T.H.Shih et al., "A new k-ε eddy-viscosity model for high Reynolds number turbulent flow", *Computers and Fluid* **24**, (3), pp.227-238, 1995